SAJSET
ISSN: 2992-3581

Savannah Journal of Science and Engineering Technology
Volume: 01; Issue: 04; Pages: 79-87; 2023.
www.sajsetjournal.com.ng

DOI: xx.xxxx.x/sajset-01-2023-0032

SAJSET
ISSN: 2992-3581

NetZero Energy Potentials of Thermoelectric Generators

[1]Saleh, U. A., [2]Yakubu, B., [3]Sulaiman, M., [3]Likoro, S. A. and [1]Ibrahim. A. S.
[1]Centre for Atmospheric Research, National Space Research and Development Agency Prince Abubakar Audu University Campus Anyigba
[2]Department of Electrical and Electronic Engineering, Federal Polytechnic, Mubi, Adamawa State
[3]Nigerian Institute of Transport Technology (NITT) Zaria.

Paper History
Received: 01st July, 2023
Accepted: 28th July, 2023
Published: August, 2023

Corresponding author
Saleh, U. A.
abubakarumarsaleh1982@gmail.com

Abstract:
The continuing rise in the cost of fossil fuels, as well as their detrimental environmental impact, has compelled researchers to look within for an alternate energy source, this brings about NetZero emissions. NetZero emissions can be attained by eliminating/minimizing greenhouse gas emissions (GHG) from the atmosphere from human activities. This paper presents the Simulation of Thermoelectric Generators Potentials for NetZero Energy Generation. Thermoelectric generators (TEG) are bi-directional devices used as coolant and energy generators. TEG have a wide application range. The simulation technique is one of the best options to evaluate thermoelectric generators' potential for NetZero energy generation. The TEG was designed using ANSYS software and the electrical energy was evaluated. The results indicate that the TEG can convert excess heat to electrical energy whenever there is a temperature gradient across the hot side and the cold side of TEG. The simulation further shows that one TEG unit can generate 1.5800 x 10^{-4} Watts.

Keywords: *ANSYS Software, Energy, Greenhouse emission, NetZero, Thermoelectric Generators*

1. Introduction

One of the big problems facing humanity soon is the increase in greenhouse emissions and minimizing its impact on the environment [1, 2]. At the same time, energy needs are rising daily [3 – 5]. The recovery of lost thermal Energy for conversion to electricity is a significant challenge for researchers and the industry [5]. TEGs will contribute to this initiative. As a growing, environmentally friendly source of ambient energy harvesting primarily through waste heat via temperature gradients, a thermoelectric generator may be the prospect of meeting energy challenges in the coming generation [6]. A solid-state system is referred to as a thermo-electric generator using the See beck effect to generate electricity. Thomas Johann See beck first detected thermo-electric phenomena in 1821. He observed the compass magnet's deflection whenever there is a temperature gradient between two dissimilar materials' junctions [7]. Indeed, such deflection is the electrical current output caused by the closed loop described by the Ampere law [8]. The closed circuit's driving current is the potential difference between hot and cold junctions for the generation of temperature gradients called the "See beck effect." The potential difference has a direct correlation with the temperature difference [9]. An intrinsic thermoelectric material property expressed in equation 1 is the See beck coefficient

$$\alpha = \frac{\Delta V}{\Delta T} \quad (1)$$

where ΔV, ΔT and α are the voltage produced, the temperature gradient and the See beck coefficient in the system [10]. This paper, therefore, presents the simulation of TEG for NetZero energy generation using Ansys simulation software.

2. Thermoelectric Generator

Thermoelectric generators as power generation are divided into two groups, namely, high power generation and low power generation [11, 12]. TEG development for low power is investigated through an environmentally friendly and cost-effective method known as direct ink [13]. The TEGs were produced on a glass substrate, the most popular insulator used in houses, and windows of two different sizes were made of poly (3, 4- ethylene dioxythiophene) polystyrene sulfonate (PEDOT: PSS) ink and silver ink materials. For TEGs with varying lengths of 30 and 40 mm at a temperature difference of 120 ^{o}C, the results indicate a maximum power of 5.17 ± 0.5 nW and 4.08 ± 0.5 nW. According to Krishna Kumar, *et al.* [14], TEG can generate power from 5 µW to 1 W with low power generation, while high power generation is considered 1 W and above. TEG is utilised as a low-power generator in biomedical, remote, and aeronautical applications [15]. Electronic devices integrated into other bodies using TEG technology for power production are classified under mobile communications. These comprise smartphones, iPods, tablets and media players. Simultaneously, others used them in the medical

sector, including hearing aids and heart pacemakers. Electronics devices incorporated in other objects have power specifications of 5 μW to 1 W [16]. Marchenko [17] presented the development and optimization of a low-temperature difference thermoelectric power harvester for the wireless sensor nodes on water pipelines. The thermoelectric harvester modelling, design, optimization, integration and experimental analysis to replace a 20 Ah battery for a wireless water quality sensor located on a water pipe was done by [18] using MATLAB software. The results indicate that the thermoelectric harvester generates more than 0.5-2 mW at a temperature gradient of around 1-2 K at a wind speed of about 1 m/s between the pipe surface and the ambient air.

2.1 Application of Thermoelectric Generator

In a wide range of applications, TEG is used in areas like wireless sensor networks [18, 19] micropower generation [20], space power [21] automotive waste heat recovery [21, 22]. Also, it can be used in wearable sensors [23-26]. A thermoelectric device is used as a means of cooling electronics equipment [27], and also in refrigerators and air conditioning systems. Specific applications for aeronautics, military, medicine, instruments, biological weapon, and other industrial products [28] and buildings [29].

2.2 Fundamental Equations for Thermoelectric Energy Conversion

Figure 1 presents the schematic diagram of the thermoelectric generator system. The system consists of a TEG hot side attached to the shingle's backside and a heatsink placed at the cold side of the TEG. Figure 2 shows its equivalent circuit diagram with a load resistance R connected across the terminal.

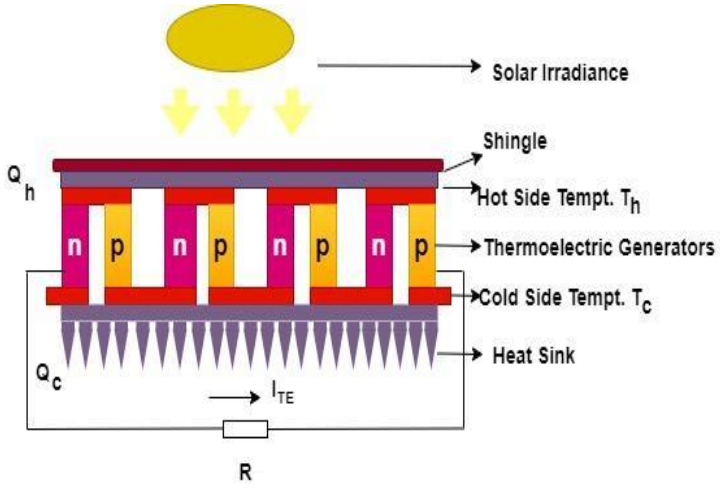

Figure 1. Schematic Diagram of Thermoelectric Generator System [30]

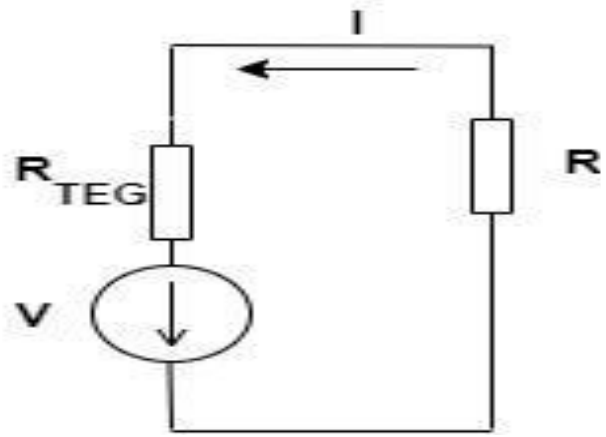

Figure 2. Equivalent Thermoelectric Generator Circuit

The voltage V through the load resistance R is in equation 2

$$V_R = IR \quad (2)$$

Where: R_{TEG} and I, are the internal resistance of the TEG and the current through the resistance. The current (I) is obtained as in equation 3

$$\mathrm{I} = \frac{\alpha(T_h - T_c)}{R + R_2} \quad (3)$$

Equations 4 and 5 shows the TEG output power

$$P = IV = \frac{\alpha^2}{(R_{TEG} + R_2)} \Delta T^2 R_{TEG} \quad (4)$$

$$P = Q_h - Q_c \quad (5)$$

Where P is the difference between the thermal Energy from the hot side to the cold side of the TEG [37]

$$Q_h = \alpha T_h I + K(T_h - T_c) - \frac{1}{2} I^2 R \quad (6)$$

$$Q_c = \alpha T_c I + K(T_h - T_c) - \frac{1}{2} I^2 R \quad (7)$$

Where $Q_h, Q_c, T_h, and\ T_c$ are the thermal Energy of the TEG hot side and cold side to the heat sink, hot side and cold side temperature of the TEG [30].

Equations 8 to 13 give the Polynomial representations for temperature-dependent properties of air and copper and temperature-dependent for the thermoelectric characteristics of n-type and p-type

$$K_n = 0.0000334545T2 - 0.023350303T + 5.606333 \quad (8)$$

$$\rho_n = (0.015601732T^2 - 15.708052T + 4466.38095)e^2 \quad (9)$$

$$\alpha_n = (0.001530736T^2 - 1.08058874T - 28.338095e^{-6} \quad (10)$$

Where Kn, ρn and αn from equations 8 to 10 are the thermal conductivity, electrical resistivity and See beck coefficient of the n-type semiconductor material of the TEG [31].

$$K_p = 0.0000361558T^2 - 0.026351342T + 6.22162 \quad (11)$$

$$\rho_p = 0.01057143T^2 - 10.16048T + 3113.71429).e^2 \quad (12)$$

$$\alpha_p = (-0.003638095T^2 + 2.74380952T - 296.214286).e^{-6} \quad (13)$$

Where K_p ρ_p and α_p from equations 11 to 13 are the thermal conductivity, electrical resistivity and See beck coefficient of p-type semiconductor material of the TEG [31].

3. Methodology

The TEG performance was evaluated using ANSYS simulation software. The software was used for the electromagnetic, thermal, and thermoelectric thermal analysis. The TEG steady-state evaluation, which enables the system's geometric modelling and several simulations inside the TEG module, including current density, temperature distribution, electric voltage, and heat flow, was carried out via ANSYS Workbench. The simulation involves three fundamental processes that consist of the following phases: Pre-processing, Solving and Post-processing. The Pre-processing phase consists of five stages [31]:

1. Modelling of the 3D using the ANSYS Modeler to construct the model geometry (Figure 3)
2. Selecting the Thermal-electric for TEG modelling
3. Inputting of the TEG engineering data
4. The building of a solid-state model that allows field temperature evaluation
5. Generation of the net finite element by ANSYS Meshing (Figure 4)

Based on direct TEG measurements, the engineering data from the experimental findings and the datasheet, and the contact and ceramic substrates' parameters from the ANSYS library. The 3D model was developed, and the thermal boundary conditions were kept constant on the substrates T_h and T_c.

Figure 3 is the graphical presentation of the thermoelectric generator with two terminals. The entire structure is created by copper alloy and a p-type portion with thermal conductivity, isotropic resistance and See beck coefficient based on equations 8 to 13. The thermal-to-electrical power conversion efficiency of the TEG material is scientifically dependent on the following crucial materials properties: the See beck coefficient, the electrical conductivity and thermal conductivity, which are expressed collectively in terms of a dimensionless figure-of-merit [32].

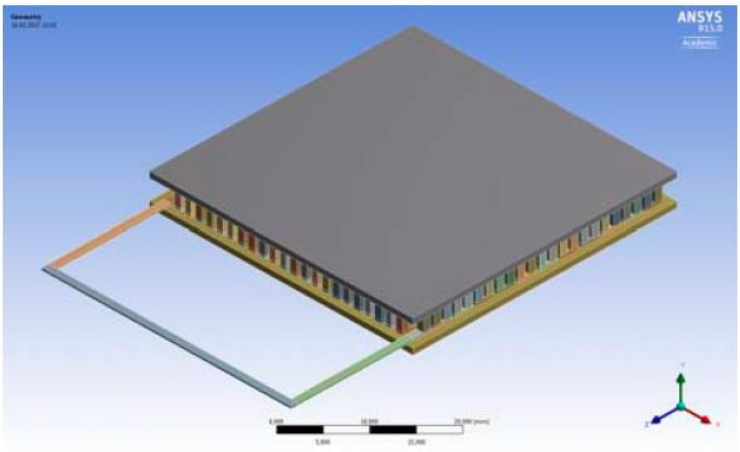

Figure 3. Thermoelectric Generator 3D Model

Figure 4 shows the meshing of the developed TEG at ANSYS. Via mesh, the entire body is divided into a number of parts to distribute the load evenly if any load is applied and automatically selects the necessary mesh in ANSYS for efficiently carrying out the built system's simulation.

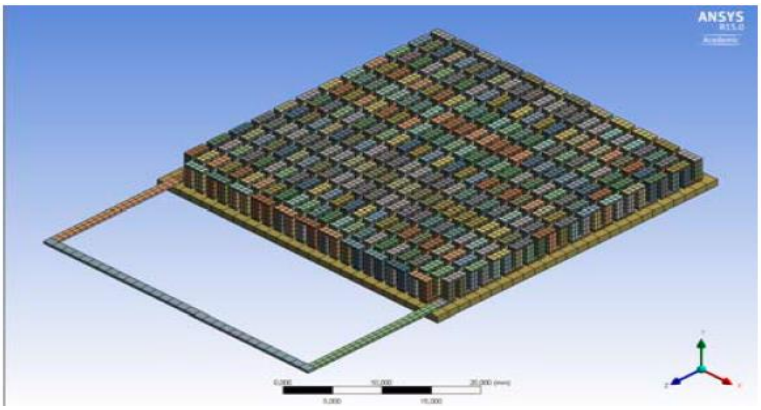

Figure 4. The Finite element model of the TEG

Figure 5 illustrates the various inputted boundary conditions. The conditions are the shingle hot side temperature as 42 ^{o}C, TEG hot side temperature as 41.5 0 C, TEG cold side temperature as 39.5 ^{o}C and the low potentials been 0V.

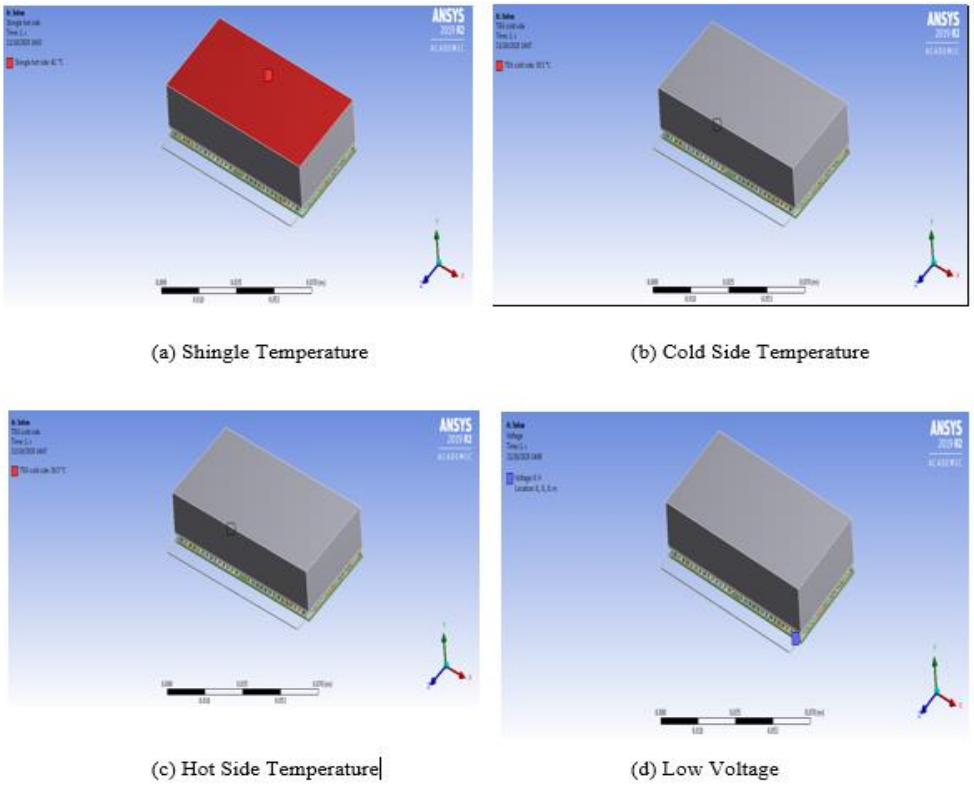

Figure 5. Inputted Boundary Conditions, (a) the Shingle Temperature, (b) Cold and (c) Hot Side Temperature, (d) Low Voltage

4. Result and Discussions

This section discussed the results of the ANSYS simulation of the thermoelectric generator. The results are displayed in shown in the screenshot from the software interface.

4.1 Results of ANYSY Simulation

For the TEG performance, this section presents the research results of the ANSYS simulation. Figure 6 shows the temperature profile of the TEG module. The red and blue colour areas indicate higher temperatures and lower temperatures, respectively. As a result, the hot junction has a higher temperature, and the cold side junction has a lower temperature [33]. The maximum temperature is 27.575 °C, while the minimum temperature is 26.109 °C.

The current density across the entire TEG unit is shown in Figure 7, and a minimum current density of 3.076 A/m^2, with a maximum density of 1730 A/m^2. Essentially, the electron flows from the n-type to the p-type element. As the temperature gradient changes between hot and cold junctions, the current density also significantly changed.

Figure 8 depict the voltage across TEG, which is as a result of the temperature gradient between the hot and cold side of the TEG.

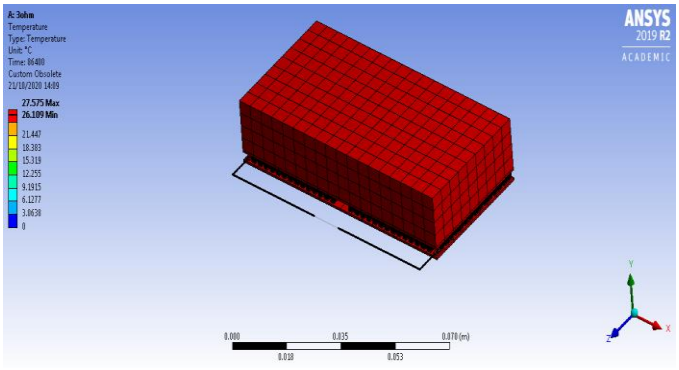

Figure 6. The temperature profile of the designed TEG

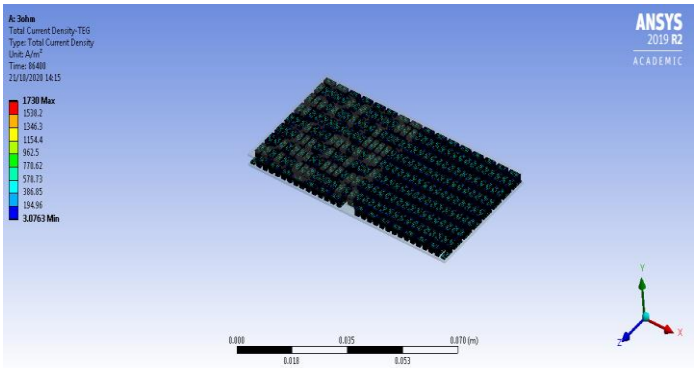

Figure 7. Current Density of the designed TEG

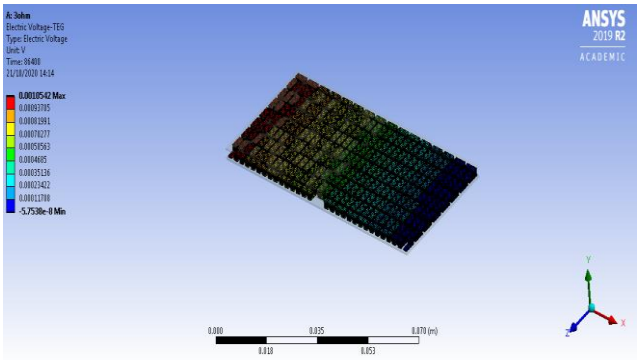

Figure 8. The voltage of the designed TEG

4.2 Temperature and the Power Output

Figures 9 to 13 below illustrated the TEG temperature profile and the output power via the Ansys simulation. The results also discussed the effect of the TEG load resistance extensively. Figure 9 depicts the hot and cold junction temperature Profile of the TEG variation for April 2020, for the hot side, the temperature varies with an increase in the solar irradiance.

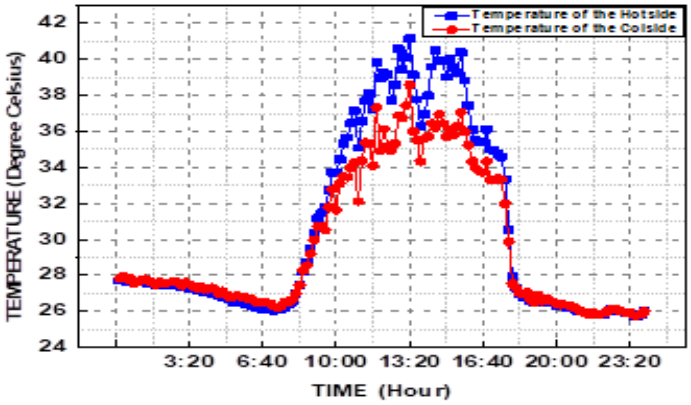

Figure 9 the variation of the hot side temperature and the cold side temperature of the TEG

At midnight the temperature was observed to be 27.745 °C it maintained the same pattern till around 8 am where it started going up with an increase in the sunshine. The result also shows a maximum temperature of 41.15 °C at around 1 pm, which resulted from high solar irradiance. The hot side is attached directly to the shingle. As the solar irradiance drop, the temperature also dropped. For the cold side, the temperature also fluctuates with the increase in the irradiance but a heatsink attached to the cold side provide cooling for the cold side to achieve a high-temperature difference between the hot and cold side.

Figure 10 illustrates the ΔT of the TEG for April. The variation was at three intervals in the day-night, morning and afternoon. During the night time, 2:10 am to 9:30 am; the system achieved a temperature difference of 0.01309 ◦C to 0.9210 ◦C. During the morning from 9:40 am to 5:30 pm a temperature difference of 0.9210 ◦C to 1.344 ◦C was reached and during the afternoon between 5:30 pm to 12 am, the system achieves a temperature difference of 1.344 ◦C to 0.0202 ◦C respectively. A maximum delta T of 4.043 ◦C was achieved at 11:50 am.

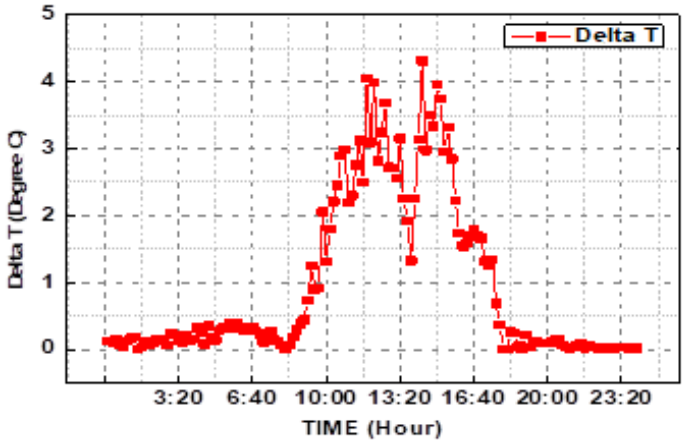

Figure 10. TEG Temperature difference (ΔT)

4.3 Results of Voltage

Figure 11 shows the voltage variations with an increase in the temperature over hourly for a 24hours time interval. The voltage measurement range was classified into three times during the night, morning, and evening time for the TEG temperature changes for the See beck coefficient. At night, the minimum voltage occurred when delta T is less than one (0.13^{O}C) was midnight (2.2660 x 10^{-3} V), at precisely 06:50 in the morning when delta T was (0.28^{O}C) the TEG produced a maximum voltage of 1.77 x 10^{-2} V. During the day at 12:10 with delta T greater than one (4.3^{O}C), the TEG has a maximum voltage of (1.3673 x 10^{-1}V) it maintains that pattern till around 17:40 the voltage changes to be (1.3176 x 10^{-1}V) and the delta was (0.69 ^{O}C)

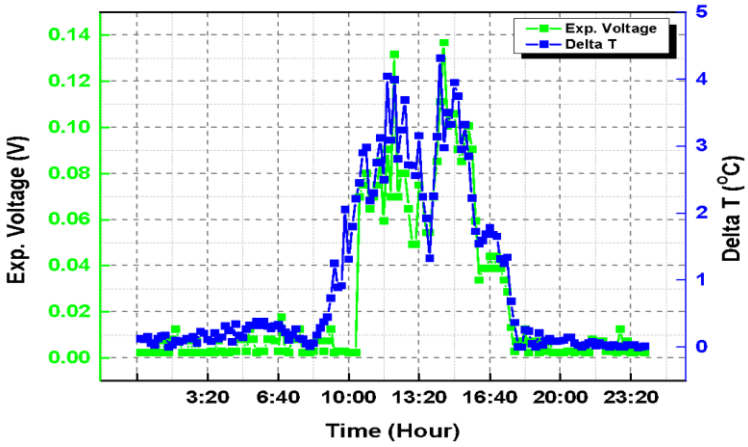

Figure 11. Output Power of TEGs

4.4 Results of Power

Figure 12 depicts the variation was divided into three times in a day as night, morning and afternoon of April 2020. During the night, the results show an output power of 4.2936 x 10^{-9} W to 2.4532 x 10^{-6} W at 12:10 am to 9:30 am. During the morning from 9:40 am to 5:30 pm, an output power of 8.5685 x 10^{-7}◦ W to 1.5800 x 10^{-4} W was reached and during the afternoon between 5:30 pm to 12 am, the result shows an output power of 9.1892 x 10^{-9} W to 1.3545x 10^{-6} W were achieved, respectively. Maximum power output was obtained at 11:50 am.

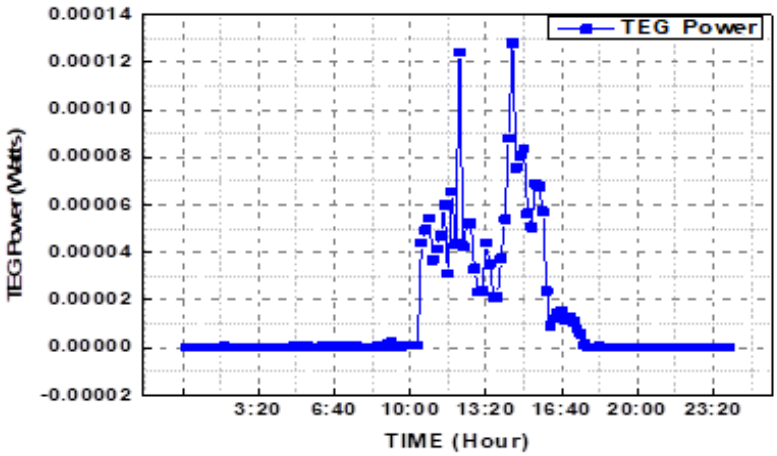

Figure 12. Output Power of TEGs.

Figure 13 shows the variation of the output power to the load. Based on the graph, the optimal power occurred at a load of 3 ohms. The results show that the load resistance is equal to the number of p and n-type semiconductor legs, equivalent to the internal electrical resistance.

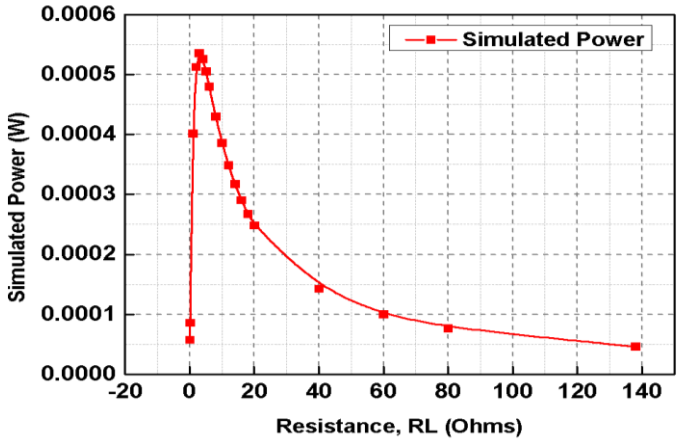

Figure 13: Variation of the TEG Simulated Output Power and the Load Resistance R_2

5. Conclusion

The simulation results have shown a practical approach to TEG physics research. In particular, it allows the efficient use of TEG as a cooling device and ambient energy generator. It will also play a significant role in hybrid system formation with photovoltaic panels for improved energy generation and increased lifespan. It will lead to the TEGs in large-scale production to the end-user in terms of power and temperatures at the specified load resistance.

Acknowledgements

The authors appreciate the Centre for Atmospheric Research for providing the needed support in conducting the Research.

Reference

[1] Ahsan, N., (2020). Solar panel size for a single-family house. *Proceedings of the International Conference on Industrial Engineering and Operations Management*, *August 2020,* North America, USA 45 2694–2699.

[2] Al Musleh, M., Topriska, E. V., Jenkins, D., and Owens, E., (2020). Thermoelectric generator characterisation at the extra-low-temperature difference for building applications in extremely hot climates: Experimental and numerical study. *Energy and Buildings*, *225*, 110285. https://doi.org/10.1016/j.enbuild.2020.110285

[3] Aljaghtham, M., and Celik, E., (2020). Design optimization of oil pan thermoelectric generator to recover waste heat from internal combustion engines. *Energy*, *200*, 117547. https://doi.org/10.1016/j.energy.2020.117547

[4] Barry, M. M., Agbim, K. A., Rao, P., Clifford, C. E., Reddy, B. V. K. and Chyu, M. K., (2016). Geometric optimization of thermoelectric elements for maximum efficiency and power output. *Energy*, *112*, 388–407. https://doi.org/10.1016/j.energy.2016.05.048

[5] Cai, Y., Wang, W. W., Liu, C. W., Ding, W. T., Liu, D. and Zhao, F. Y., (2020). Performance evaluation of a thermoelectric ventilation system driven by the concentrated photovoltaic, thermoelectric

generators for green building operations. *Renewable Energy*, *147*, 1565–1583. https://doi.org/10.1016/j.renene.2019.09.090

[6] Cai, Y., Wang, Y., Liu, D., and Zhao, F. Y. (2019). Thermoelectric cooling technology applied in the field of electronic devices: Updated review on the parametric investigations and model developments. *Applied Thermal Engineering*, *148*(April 2018), 238–255. https://doi.org/10.1016/j.applthermaleng.2018.11.014

[7] Cekdin, C., Nawawi, Z., and Faizal, M. (2020). The usage of thermoelectric generator as a renewable energy source. *Telkomnika (Telecommunication Computing Electronics and Control)*, *18*(4), 2186–2192. https://doi.org/10.12928/TELKOMNIKA.V18I4.13072

[8] Chintha, S. (2019). Experimental investigations on thermoelectric power generation from wastage. *Energies* , xi(*xii*), 90–93.

[9] Elghool, A., Basrawi, F., Ibrahim, T. K., Ibrahim, H., Ishak, M., Hazwan, Yusof. M. and Bagaber, S. A., (2020). Multi-objective optimization to enhance the performance of thermo-electric generator combined with heat pipe-heat sink under forced convection. *Energy*, *208*, 118270. https://doi.org/10.1016/j.energy.2020.118270

[10] Hamid Elsheikh, M., Shnawah, D. A., Sabri, M. F. M., Said, S. B. M., Haji Hassan, M., Ali Bashir, M. B. and Mohamad, M., (2014). A review on thermoelectric renewable Energy: Principle parameters that affect their performance. *Renewable and Sustainable Energy Reviews*, *30*, 337–355. https://doi.org/10.1016/j.rser.2013.10.027

[11] Hussain Shah, W. and Muhammad Khan, W., (2020). Thermoelectric Properties of Chalcogenide System. *Electromagnetic Field Radiation in Matter*, *145(47)*, 1–20. https://doi.org/10.5772/intechopen.93248

[12] Khanmohammadi, S., Musharavati, F., Kizilkan, O., and Duc Nguyen, D., (2020). Proposal of a new parabolic solar collector-assisted power-refrigeration system integrated with a thermoelectric generator using 3E analyses: Energy, exergy, and energy-economic. *Energy Conversion and Management*, *220*, 113055. https://doi.org/10.1016/j.enconman.2020.113055

[13] Kishore, R. A., Nozariasbmarz, A., Poudel, B. and Priya, S., (2020). High-Performance Thermoelectric Generators for Field Deployments. *ACS Applied Materials and Interfaces*,*12*(9), 10389–10401. https://doi.org/10.1021/acsami.9b21299

[14] Krishna Kumar, T. S., Anil Kumar, S., Kodanda Ram, K., Raj Goli, K. and Siva Prasad, V., (2020). Analysis of thermoelectric generators in automobile applications. *Materials Today: Proceedings of the Second International Conference on energy systems (IES-II), Madagasca 70(23) June 13-17, 2020*. https://doi.org/10.1016/j.matpr.2020.08.081

[15] Lineykin, S., Sitbon, M. and Kuperman, A., (2020). Design and optimization of low-temperature gradient thermoelectric harvester for wireless sensor network node on water pipelines. *Applied Energy*, *20(8)* 116240. https://doi.org/10.1016/j.apenergy.2020.116240

[16] Lund, A., Tian, Y., Darabi, S. and Müller, C., (2020). A polymer-based textile thermoelectric generator for wearable energy harvesting. *Journal of Power Sources*, *480*, 228836. https://doi.org/10.1016/j.jpowsour.2020.228836

[17] Marchenko, O., (2020). Energy and economic analysis of thermoelectric generator on wood fuel. *E3S Web of Conferences*, *209*, 03017. https://doi.org/10.1051/e3sconf/202020903017

[18] Miao, Z., Meng, X., Zhou, S. and Zhu, M., (2020). Thermo-mechanical analysis on thermoelectric legs arrangement of thermoelectric modules. *Renewable Energy*, *147*, 2272–2278. https://doi.org/10.1016/j.renene.2019.10.016

[19] Mirzakhanyan, A., (2005). Economic and social development. *The Armenians: Past and Present in the Making of National Identity*, *3*, 196–210. https://doi.org/10.4324/9780203004937

[20] Patel, V. R. and Patel, M. C., (2020). Automobile Waste Heat Recovery System Using Thermoelectric Generator. *Journal of Science and Technology*, *5*(3), 58–61. https://doi.org/10.46243/jst.2020.v5.i3.pp58-61

[21] Rana, S., Orr, B., Iqbal, A., Ding, L. C., Akbarzadeh, A. and Date, A., (2017). Modelling and Optimization of Low-temperature Waste Heat Thermoelectric Generator System. *Energy Procedia*, *110*, 196–201. https://doi.org/10.1016/j.egypro.2017.03.127

[22] Rostamzadeh, H. and Nourani, P., (2019). Investigating potential benefits of a salinity gradient solar pond for ejector refrigeration cycle coupled with a thermoelectric generator. *Energy*, *172*, 675–690. https://doi.org/10.1016/j.energy.2019.01.167

[23] Sahin, A. Z., Ismaila, K. G., Yilbas, B. S. and Al-Sharafi, A., (2020). A review of the performance of photovoltaic/thermoelectric hybrid generators. *International Journal of Energy Research*, 10(2) 1–30. https://doi.org/10.1002/er.5139

[24] Saleh, U. A., Haruna, Y. S., Gwaram, U. A. and Abu, U. A.. (2018). Evaluation of Solar Energy Potentials for Optimized Electricity Generation at Anyigba, North Central Nigeria. *Global Scientific Journals*, *6*(2), 263–270. https://www.worldenergy.org/wp-content/uploads/2016/10/World-Energy-Resources_SummaryReport_2016.10.03.pdf

[25] Saleh, U. A., Abdulrahman Sulaiman, and Haruna Y. S (2021) Performance Evaluation of some selected Mediums Wind Energy Conversion Systems for Wind Power Generation at. *Proceedings of the 2nd African International Conference on Industrial Engineering and Operations Management, Harare, Zimbabwe, December 8-10, 2020*, pp. 2578–2586, 2020.

[26] Saleh, U. A., Haruna, Y. S. and Onuigbo, F. I., (2015). *Design and Procedure for Stand-Alone*

Photovoltaic Power System for Ozone Monitor Laboratory at Anyigba, North Central. *4*(6), 41–52.

[27] Saleh, U. A., Johar, M. A., Jumaat, S. A. B., Rejab, M. N., and Wan Jamaludin, W. A., (2020). Evaluation of a PV-TEG Hybrid System Configuration for an Improved Energy Output: A Review. *International Journal of Renewable Energy Development*, *10*(2), 385–400. https://doi.org/10.14710/ijred.0.33917

[28] Saleh A. U., & Jumaat, S. A. (2022). The Hybrid Photovoltaic - Thermoelectric Generator Configurations for Energy Performance Improvement. *International Journal of Integrated Engineering*, *14*(3), 1–13

[29] Shakeel, M., Rehman, K., Ahmad, S., Amin, M., Iqbal, N. and Khan, A. (2020). A low-cost printed organic thermoelectric generator for low-temperature energy harvesting. *Renewable Energy*, Volume 167, Pages 853-860 https://doi.org/10.1016/j.renene.2020.11.158

[30] Saleh, A. U, S. A. Jumaat, Johar Muhammad Akmal & W. A. W. Jamaludin (2021). The real-time monitoring of TEG using LabVIEW Technique for Green Energy Generation. *Multidisciplinary Applied Research and Innovation (MARI)* Vol. 2 No 3, 112-116.

[31] Wang, X., Ting, D. S. K. and Henshaw, P., (2020). Mutation particle swarm optimization (M-PSO) of a thermoelectric generator in a multi-variable space. *Energy Conversion and Management*, *224*, 113387. https://doi.org/10.1016/j.enconman.2020.113387

[32] Wen, D. L., Deng, H. T., Liu, X., Li, G. K., Zhang, X. R. and Zhang, X. S., (2020). Wearable multi-sensing double-chain thermoelectric generator. *Microsystems and Nanoengineering*, *6*(1), 6-20. https://doi.org/10.1038/s41378-020-0179-6